Available online at www.sciencedirect.com
SCIENCE DIRECT®
International Journal of Heat and Mass Transfer 47 (2004) 659–669
International Journal of HEAT and MASS TRANSFER
www.elsevier.com/locate/ijhmt

Transient modeling of a two-bed silica gel–water adsorption chiller

H.T. Chua [a,b,*], K.C. Ng [b], W. Wang [b], C. Yap [b], X.L. Wang [b]

[a] Bachelor of Technology Programme, Faculty of Engineering, National University of Singapore, 9 Engineering Drive 1, Blk EA #07-32, Singapore 117576, Singapore

[b] Mechanical Engineering Department, Faculty of Engineering, National University of Singapore, Singapore 119260, Singapore

Received 25 November 2002; received in revised form 6 August 2003

Abstract

This article presents a transient distributed-parameter model for a two-bed, silica gel–water adsorption chiller. Compared with our previous lumped-parameter model, we found better agreement between our model prediction and experimental data. We discussed the important effect of heat recovery and the effect of extra system piping on the system performance. Time constants of sensors were also considered. We found that the chiller was able to maintain its cooling capacity over a fairly broad range of cycle times and the previous lumped-parameter model tended to under-predict the cooling capacity at long cycle times.

1. Introduction

Recently, adsorption chillers have been gaining more and more attention due to merits such as being environmentally friendly and having no moving parts. Fig. 1 shows the schematic of a basic two-bed adsorption chiller which represents the most basic module for this class of system. This type of chiller utilizes the uptake characteristics of adsorbent–adsorbate systems to effect useful cooling at the evaporator. Details pertaining to the operation of such a two-bed adsorption chiller could be found in the earlier literature [1,2].

In this context, silica gel–water has been selected as the adsorbent–adsorbate pair due to its relatively low regeneration temperature (below 100 °C, and typically about 85 °C). This working pair enjoys a large uptake capacity for water which in turn has a high latent heat of evaporation—typically up to 40% of the silica gel dry mass [3,14]. Many mathematical models and computer codes have been developed for adsorption chillers. The chronological development of those models presented can be classified into two main branches: (i) uniform temperature and pressure models [4–7]. Guilleminot et al. [8] considered temperature inhomogeneity and the influence of fins inside the bed, but neglected all the mass transfer resistances in the adsorbent. (ii) Detailed mathematical models which were originally proposed for adsorption heat pumps equipped with temperature wave thermal generation [9]. Such models accounted for both heat and mass transfer resistances within the adsorber. Luo and Tondeur [10] proposed a model of the adsorber unit which correctly described the transient temperature profiles within the adsorber that had been observed experimentally. However, their model ignored the mass transfer resistance at the fluid/solid interface. Zhang [11] studied an intermittent adsorption cooling system using a three-dimensional non-equilibrium model, where both internal and external mass transfer resistances within the adsorbent bed were accounted for. Furthermore, the model considered the effects of fins that intensified the heat transfer in the adsorbent bed. However, the model was considerably simplified by assuming that (i) the adsorbed phase was a liquid, (ii) the

* Corresponding author. Address: Bachelor of Technology Programme, Faculty of Engineering, National University of Singapore, 9 Engineering Drive 1, Blk EA #07-32, Singapore 117576, Singapore. Tel.: +65-874-8057; fax: +65-874-3525.
E-mail address: engcht@nus.edu.sg (H.T. Chua).

0017-9310/$ - see front matter © 2003 Elsevier Ltd. All rights reserved.
doi:10.1016/j.ijheatmasstransfer.2003.08.010

Nomenclature

COP	coefficient of performance
c_p	specific heat capacity (J/kg·K)
d	diameter (m)
D_{so}	pre-exponent constant (m^2/s)
E_a	activation energy of surface diffusion (kJ/kg)
FS	fin space (m)
h	heat transfer coefficient, specific enthalpy (W/m^2 K, J/kg)
h_{fg}	latent heat of condensation or vaporization (J/kg)
k	thermal conductivity (W/m·K)
K_0	constant in isotherm equation (kg/kg dry adsorbent/Pa)
L	length (m)
m	mass (kg)
$\dot{m}$	mass flow rate (kg/s)
P	pressure (Pa)
q	fraction of refrigerant adsorbed by the adsorbent (kg/kg dry adsorbent)
q^*	fraction of refrigerant which can be adsorbed by the adsorbent under saturation condition (kg/kg dry adsorbent)
q_∞	ultimate uptake (kg/kg dry adsorbent)
r	radius (m)
t	time, index in isotherm equation (2) (s, –)
T	temperature (°C)
u	specific internal energy, velocity (J/kg, m/s)
V	volume (m^3)
ΔH_{ads}	isosteric heat of adsorption (J/kg)
δ	fin thickness (m)
ε	porosity
μ	viscosity ($N\,s/m^2$)
ρ	density (kg/m^3)
τ	time constant (s)

Subscripts

b	bed
c	condenser
cham	chamber in the adsorption bed
chilled	chilled water
cond	condenser cooling water
cooling	cooling water
cycle	One cycle with one bed undergoing either one complete adsorption/desorption
e	evaporator
f	fluid (water)
fin	fin
heating	hot water
i	inner
in	inlet
l	liquid water, left
m	metal tube
measured	experimentally measured
o	outer
p	particle
r	radial direction, right
real	real value
s	silica gel
switching	switching stage
t	total
v	water vapor
z	axial direction

gaseous adsorbate was an ideal gas, and (iii) the condenser and the evaporator were ideal and possessed an infinite heat transfer coefficient.

Building from our previous work [1], this article systematically presents a transient distributed-parameter model which simulates the performance of a two-bed adsorption chiller. The model considered both the heat and mass transfer resistances of the adsorption bed as well as the temporal energetic behavior in the evaporator and condenser.

2. Mathematical model

In this article, we aspire to provide a detailed and practical model of a commercial adsorption chiller. In such chillers, circular fins are used for the ease of mass production. In which case, our model could be simplified by an axisymmetrical consideration. All the parameters used in the mathematical model are listed in Table 1. The main simplifying assumptions are as follows:

1. The adsorption bed is composed of uniform size particles and the bed porosity is a constant. The specific heat and the density of dry adsorbent are constant.
2. The physical properties of metal tube and fin are constant.
3. No heat losses from the adsorption/desorption bed are considered.

2.1. Adsorption equations

The adsorption rate is controlled by surface diffusion inside a particle. Sakoda and Suzuki [12] introduced a linear driving force equation to account for the mass transfer resistance within the particle that can be expressed as

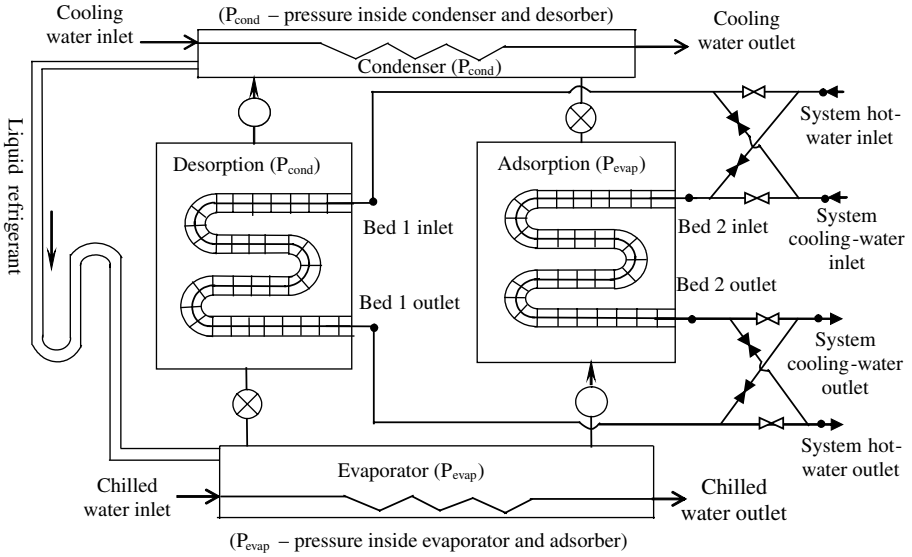

Fig. 1. Schematic of a two-bed adsorption chiller. (⋈: opened water valve; ⋈: closed water valve; ⊗: closed gas valve; ○: opened gas valve).

Table 1
Values for the parameters used in the present model

D_{s0}	2.54×10^{-4} m^2/s
E_a	4.2×10^{4} J/mol
R_p	7.1×10^{-4} m
K_0	7.3×10^{-13} kg/(kg Pa) [12]
ΔH_{ads}	2.693×10^{6} J/kg [12]
q_m	0.45 kg/kg [12]
t	12 [12]
$c_{p,m}$	386 J/(kg K)
$c_{p,fin}$	905 J/(kg K)
$c_{p,s}$	924 J/(kg K)
ρ_m	8930 kg/m^3
ρ_s	2027 kg/m^3
ρ_{fin}	2710 kg/m^3
k_m	398 W/(m K)
k_{fin}	246 W/(m K)
k_s	0.198 W/(m K)
$h_{c,o}$	5004.34 W/(m^2 K)
$h_{e,o}$	2034.13 W/(m^2 K)
$h_{fin,s}$	36 W/(m^2 K)
$h_{m,s}$	36 W/(m^2 K)
ε_t	0.64
ε_b	0.37
$T_{chilled,in}$	14.8 °C
$T_{heating,in}$	86.3 °C
$T_{cooling,in}$	31.1 °C
$\dot{m}_{cooling}$	1.52 kg/s
$\dot{m}_{heating}$	1.28 kg/s
$\dot{m}_{chilled}$	0.71 kg/s
$\dot{m}_{cond}$	1.37 kg/s
t_{cycle}	442 s
$t_{switching}$	30 s
τ	15 s

$$\frac{\partial q}{\partial t} = 15 D_{so}\exp(-E_a/RT_s)/R_p^2\cdot(q^*-q), \tag{1}$$

where q^* is the equilibrium uptake at (T_s, P_s).

Equilibrium water uptake q^* is expressed by the adsorption-equilibrium equations. In this context, Tóth equation [13] is used as follow

$$q^* = \frac{K_0\exp\{\Delta H_{ads}/(R\cdot T)\}P}{[1+\{K_0/q_\infty\cdot\exp(\Delta H_{ads}/(R\cdot T))\cdot P\}^t]^{1/t}}, \tag{2}$$

where q_∞, K_0 and t are constants.

2.2. Thermodynamic properties of water and steam

In this context, all the thermodynamic properties of water and steam are calculated according to the formulation offered by Wagner and Kruse [15].

2.3. Chiller system modeling

On account of the circular structure of adsorption bed, all the equations are written in cylindrical coordinates.

2.3.1. Adsorption bed

2.3.1.1. Silica gel. The overall mass conservation in the porous bed is described as

$$\int_V\left[\varepsilon_t\frac{\partial\rho_v}{\partial t}+(1-\varepsilon_t)\rho_s\frac{\partial q}{\partial t}\right]dV = \dot{m}_{e/c,v} \tag{3}$$

where

$$\varepsilon_t = \varepsilon_b + (1-\varepsilon_b)\varepsilon_p.$$

The energy balance on the control volume (adsorbent + adsorbate + inter-particle vapor) can be written as

$$(1-\varepsilon_t)\left[\rho_s c_{p,s}\frac{\partial T_s}{\partial t}+\rho_s(h_g-\Delta H_{ads})\frac{\partial q}{\partial t}+\rho_s q c_{p,g}\frac{\partial T_s}{\partial t}\right]+\varepsilon_t\frac{\partial(\rho_v u_v)}{\partial t}$$
$$=\frac{\partial\left(k_s\frac{\partial T_s}{\partial r}r\right)}{r\partial r}+\frac{h_{fin,s}}{FS}(T_{fin,l}-T_s)-\frac{h_{fin,s}}{FS}(T_s-T_{fin,r}). \quad (4)$$

Temperature boundary conditions

$$-k_s\frac{\partial T_s}{\partial r}|_{r=r_o}=h_{m,s}(T_m-T_s), \quad (5)$$

$$\frac{\partial T_s}{\partial r}|_{r=r_{fin}}=0. \quad (6)$$

Pressure boundary conditions

$$P_s=P_c \quad \text{when being connected to the condenser,} \quad (7)$$

$$P_s=P_e \quad \text{when being connected to the evaporator,} \quad (8)$$

$$P_s=P_{cham} \quad \text{during switching time.} \quad (9)$$

P_{cham} can be determined by the mass balance and energy balance equations which can be expressed as follow:

Mass balance equation

$$\frac{d\rho_{cham}}{dt}=-\frac{1}{V_{cham}}\int_{V_b}\left[\varepsilon_t\frac{\partial\rho_v}{\partial t}+(1-\varepsilon_t)\rho_s\frac{\partial q}{\partial t}\right]dV. \quad (10)$$

Energy balance equation

$$\frac{d(\rho_{cham}u_{cham})}{dt}=-\frac{1}{V_{cham}}\left[\varepsilon_t\frac{\partial(\rho_v u_v)}{\partial t}+(1-\varepsilon_t)\rho_s\frac{\partial q}{\partial t}\right]dV. \quad (11)$$

2.3.1.2. Fins. The fin thickness is very small and the heat transfer in the fin is assumed to be one dimensional in the radial direction.

The energy balance equation of the control volume in the fin is

$$\delta\rho_{fin}c_{p,fin}\frac{\partial T_{fin}}{\partial t}=k_{fin}\delta\frac{\partial\left(\frac{\partial T_{fin}}{\partial r}r\right)}{r\partial r}+h_{fin,s}(T_{s,l}-T_{fin})-h_{fin,s}(T_{fin}-T_{s,r}). \quad (12)$$

Temperature boundary conditions

$$T_{fin}|_{r=r_o}=T_m, \quad (13)$$

$$\frac{\partial T_{fin}}{\partial r}|_{r=r_{fin}}=0. \quad (14)$$

2.3.1.3. Metal tube

$$\rho_m c_{p,m}\frac{\partial T_{b,m}}{\partial t}(r_o^2-r_i^2)=k_m\frac{\partial^2 T_{b,m}}{\partial z^2}(r_o^2-r_i^2)+2r_i h_{f,m}(T_f-T_{b,m})-2r_o h_{m,s}(T_{b,m}-T_s)+2(1-\xi)r_o k_{fin}\frac{\partial T_{fin}}{\partial r}. \quad (15)$$

When fin is involved $\xi=0$, otherwise $\xi=1$.

Temperature boundary conditions

$$\frac{\partial T_{b,m}}{\partial z}|_{z=0}=\frac{\partial T_{b,m}}{\partial z}|_{z=L}=0. \quad (16)$$

2.3.1.4. Cooling water/hot water. Since $r_i/L_b\ll 1$, the heat transfer in the fluid is assumed one dimensional (in axial direction). Energy balance on the cooling water control volume can be written as

$$\rho_f c_{p,f}\frac{\partial T_f}{\partial t}=-u_f\rho_f c_{p,f}\frac{\partial T_f}{\partial z}+\frac{\partial}{\partial z}\left(k_f\frac{\partial T_f}{\partial z}\right)-\frac{2h_{f,m}}{r_i}(T_f-T_{b,m}), \quad (17)$$

where $h_{f,m}$ is calculated with the aid of the Dittus–Boelter correlation for smooth tube.

Temperature boundary conditions

$$T_f|_{z=0}=T_{cooling,in} \quad \text{when cooling,} \quad (18)$$

$$T_f|_{z=0}=T_{hot,in} \quad \text{when heating,} \quad (19)$$

$$\frac{\partial T_f}{\partial z}|_{z=L_b}=0. \quad (20)$$

2.3.2. Condenser

2.3.2.1. Metal tube. The energy balance equation of the condenser tube control volume can be expressed as:

$$\rho_m c_{p,m}\frac{\partial T_{c,m}}{\partial t}\frac{d_{c,o}^2-d_{c,i}^2}{4}=k_m\frac{\partial^2 T_{c,m}}{\partial z^2}\frac{(d_{c,o}^2-d_{c,i}^2)}{4}-d_{c,i}h_{c,i}(T_{c,m}-T_{cooling})+d_{c,o}h_{c,o}(T_c-T_{c,m}). \quad (21)$$

Temperature boundary conditions

$$\frac{\partial T_{c,m}}{\partial z}|_{z=0}=0, \quad (22)$$

$$\frac{\partial T_{c,m}}{\partial z}|_{z=L_c}=0. \quad (23)$$

2.3.2.2. Cooling water. Energy balance equation on the cooling water control volume

$$\rho_f c_{p,f}\frac{\partial T_{cooling}}{\partial t}=-u_{cooling}\rho_f c_{p,f}\frac{\partial T_{cooling}}{\partial z}+\frac{\partial}{\partial z}\left(k_f\frac{\partial T_{cooling}}{\partial z}\right)-\frac{4h_{c,i}}{d_{c,i}}(T_{cooling}-T_{c,m}). \quad (24)$$

Temperature boundary conditions

$$T_{cooling}|_{z=0}=T_{cooling,in}, \quad (25)$$

$$\frac{\partial T_{cooling}}{\partial z}|_{z=L_c}=0. \quad (26)$$

2.3.2.3. Water vapor in the condenser

a. *Switching period*
Mass balance equation

$$\frac{\mathrm{d}\rho_{\mathrm{v,c}}}{\mathrm{d}t}V_{\mathrm{c}} = -\dot{m}_{\mathrm{c}}. \tag{27}$$

Energy balance equation

$$\frac{\mathrm{d}(\rho_{\mathrm{v,c}}u_{\mathrm{v,c}})}{\mathrm{d}t}V_{\mathrm{c}} = -\dot{m}_{\mathrm{c}}h_{\mathrm{v,c}}, \tag{28}$$

where V_{c} is the volume of the empty space in the condenser.

b. *Normal operation period*
We assume that all the water vapor coming from the desorption bed can be condensed on the condenser tube. Therefore, the condensing temperature can be determined by an iterative method.

2.3.3. Evaporator

2.3.3.1. Metal tube. Energy balance equation

$$\rho_{\mathrm{m}}c_{p,\mathrm{m}}\frac{\partial T_{\mathrm{e,m}}}{\partial t}\frac{(d_{\mathrm{e,o}}^2-d_{\mathrm{e,i}}^2)}{4} = k_{\mathrm{m}}\frac{\partial^2 T_{\mathrm{e,m}}}{\partial z^2}\frac{(d_{\mathrm{e,o}}^2-d_{\mathrm{e,i}}^2)}{4} + d_{\mathrm{e,i}}h_{\mathrm{e,i}}(T_{\mathrm{chilled}}-T_{\mathrm{e,m}}) - d_{\mathrm{e,o}}h_{\mathrm{e,o}}(T_{\mathrm{e,m}}-T_{\mathrm{e}}). \tag{29}$$

Temperature boundary conditions

$$\frac{\partial T_{\mathrm{e,m}}}{\partial z}\Big|_{z=0} = 0, \tag{30}$$

$$\frac{\partial T_{\mathrm{e,m}}}{\partial z}\Big|_{z=L_{\mathrm{e}}} = 0. \tag{31}$$

2.3.3.2. Chilled water. Energy balance equation on the fluid control volume

$$\rho_{\mathrm{f}}c_{p,\mathrm{f}}\frac{\partial T_{\mathrm{chilled}}}{\partial t} = -u_{\mathrm{chilled}}\rho_{\mathrm{f}}c_{p,\mathrm{f}}\frac{\partial T_{\mathrm{chilled}}}{\partial z} + \frac{\partial}{\partial z}\left(k_{\mathrm{f}}\frac{\partial T_{\mathrm{chilled}}}{\partial z}\right) - \frac{4h_{\mathrm{e,i}}}{d_{\mathrm{e,i}}}(T_{\mathrm{chilled}}-T_{\mathrm{e,m}}). \tag{32}$$

Temperature boundary conditions

$$T_{\mathrm{chilled}}|_{z=0} = T_{\mathrm{chilled,in}}, \tag{33}$$

$$\frac{\partial T_{\mathrm{chilled}}}{\partial z}\Big|_{z=L_{\mathrm{e}}} = 0. \tag{34}$$

2.3.3.3. Refrigerant in evaporator. We assume that the refrigerant inside the evaporator is in a saturated state.

Mass balance equation on the refrigerant outside the evaporator tube.

$$\frac{\mathrm{d}m_{\mathrm{e}}}{\mathrm{d}t} = \dot{m}_{\mathrm{c}} - \dot{m}_{\mathrm{e,v}}. \tag{35}$$

Energy balance equation on the refrigerant outside the evaporator tube.

$$\frac{\partial(m_{\mathrm{e}}u_{\mathrm{e}})}{\partial t} = \dot{m}_{\mathrm{c}}h_{\mathrm{c}} - \dot{m}_{\mathrm{e,v}}h_{\mathrm{v}} + \int_0^{L_{\mathrm{e}}} h_{\mathrm{e,o}}\pi d_{\mathrm{e,o}}(T_{\mathrm{e,m}}-T_{\mathrm{e}})\,\mathrm{d}z. \tag{36}$$

2.3.3.4. Effect of the temperature-sensor time constant on the measured temperatures

$$\frac{\mathrm{d}T_{\mathrm{measured}}}{\mathrm{d}t} = \frac{1}{\tau}(T_{\mathrm{real}}-T_{\mathrm{measured}}). \tag{37}$$

The set of partial differential equations developed above was numerically solved using the finite difference method. The whole computational domain was discretized and divided into a number of equal step discrete elements (N_r in the radial direction and N_z in the axial direction). Since the fin thickness and spacing between the fins are very small, a number of adjoining fins and the corresponding silica gel masses are separately treated as two interacting control volumes, each having its own spatial and temporal temperature and mass (in the case of the silica gel masses) distribution. The temperature difference between these two control volumes is dictated by the representative interfacial thermal contact resistance between the fin and adjoining silica gel (see Fig. 2). N_r and N_z were set to 3 and 10 respectively. The diffusion terms in the equations were approximated by a central difference scheme and the convection terms were replaced by an upstream difference scheme. Finally, a set of coupled ordinary differential equations was obtained and solved using the fifth-order Gear's backward differentiation formulae method. Double precision was used and the tolerance set to 1×10^{-6}. A mesh test has been carried out and no obvious difference can be found after further refining the mesh size. Once the initial conditions are given, the program computes from transient to cyclic-steady-state conditions. In the case of a typical operating condition, using a Pentium III 700

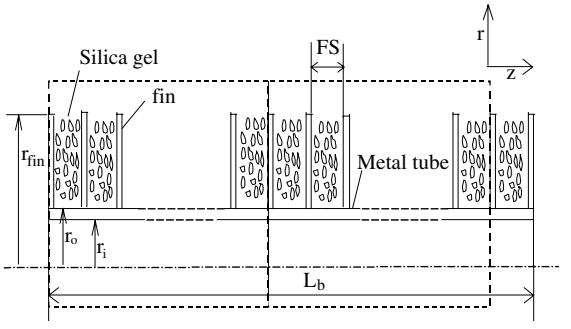

Fig. 2. Schematic of the control-volume selection of a section of an adsorption bed.

MHz, 128 Mbytes personal computer is sufficient for the requisite computation.

The cycle averaged cooling power, Q_{evap} and COP are useful yardsticks for the designer, and a convenient way for the manufacturer to describe its product. Q_{evap} and COP are respectively defined as:

$$Q_{\text{evap}} = \dot{m}_{\text{chilled}}[c_{p,\text{f}}(T_{\text{chilled,in}})]\int_0^{t_{\text{cycle}}}(T_{\text{chilled,in}} - T_{\text{chilled,out}})\,\mathrm{d}t, \tag{38}$$

$$\text{COP} = \frac{Q_{\text{evap}}}{\dot{m}_{\text{heating}}[c_{p,\text{f}}(T_{\text{heating,in}})]\int_0^{t_{\text{cycle}}}(T_{\text{heating,in}} - T_{\text{heating,out}})\,\mathrm{d}t}. \tag{39}$$

3. Results and discussion

We have performed some consistency checks and confirmed that irregardless of the initial refrigerant mass distribution, our model is able to achieve the same cyclic-steady-state within five cycles. We have also checked that the energy imbalance between the sum of cooling capacity and desorber heat input as well as the sum of condenser and adsorber heat rejections is about 1–2%.

3.1. Comparison with cyclic-steady-state experimental data

The current formulation represents an improvement to the models of Saha et al. [16] and Chua et al. [1]. The data presented here are considered under the standard operating condition. In the model the total refrigerant inventory has been chosen to be 68.9 kg. The comparison of predicted and experimentally measured outlet temperatures is shown in Fig. 3. One can observe that the current prediction agrees much better with the experimental measurements than our previous model [1]. The predicted cooling capacity and COP are 10.7 kW and 0.38, respectively while the experimental cooling capacity and COP are 10.7 kW and 0.39 respectively. It is imperative to note that the measured outlet temperatures of the beds are affected by the time constant of the temperature sensors. The temperatures shown in Fig. 3 are the system outlet temperatures which are different from those of the beds. The schematic location of these temperature points, viz. the system outlet temperature and bed outlet temperature points, is shown in Fig. 1. Hence, the system hot-water inlet and outlet points trace the hot-water supply and return temperatures while the system cooling-water inlet and outlet points trace the cooling-water supply and return temperatures. In contrast, the beds inlet and outlet temperature points respectively trace the incoming and outgoing fluid temperatures as experienced by the beds. Depending on the particular process state in a cycle, the fluid could be hot water or cooling water. Fig. 4 shows the difference between the beds and system outlet temperatures. This difference is essentially due to the heat capacities of the beds, the piping and the fluids carried by the piping. Starting from the instance at which bed switching begins, the relatively cool water emanating from the bed that is being switched to a desorber still leaves the system via the system cooling-water outlet as this fluid is still cooler than the fluid that emanates from the bed that is being switched to an adsorber. Concomitantly, the relatively warm water emanating from the bed that is being switched to an adsorber leaves via the system hot-water outlet. This process flow scheme continues until the temperatures of the waters leaving the two beds equate. In our present context, this water diversion process lasts for 15 s. Thereafter, the water emanating from the adsorber leaves via the system cooling-water outlet while that emanating from the desorber leaves via the system hot-water outlet. This flow scheme results in an energetically more efficient system compared with an arrangement whereby the water emanating from the adsorber is strictly sent to the system cooling-water outlet while the water emanating from the desorber is strictly channeled to the system hot-water outlet. Hence, the flow scheme that we have studied in this article is effectively a thermally regenerative scheme that recovers the energy of the hot adsorber and its associated piping.

3.2. Dühring diagram of the cyclic-steady-state condition of the beds

Fig. 5 presents the simulated Dühring diagram of the cyclic-steady-state condition of an entire bed. From Fig. 5, one observes that during the cold-to-hot thermal swing of the bed, although the hot water is already applied, momentary adsorption still takes place at the inception. Here, the average temperature refers to the average of the summation of all nodal temperature points of the silica gel. The entire bed is observed to be essentially following an isosteric path during switching. In contrast, the local spatial points in the bed are not evolving in an isosteric manner. This is confirmed by our simulation. This goes to show that while some parts of the bed may continue to adsorb, other parts desorb, resulting in the entire bed following an isosteric path. At the end of the hot-to-cold thermal swing, there is a pressure drop in the bed pressure. This causes the adsorbate in the cool bed to desorb momentarily and condense into the evaporator. The switching time set by the manufacturer is somewhat short for the beds to change to the expected pressures. This design is due to the consideration of the maximum cooling capacity that we will discuss later.

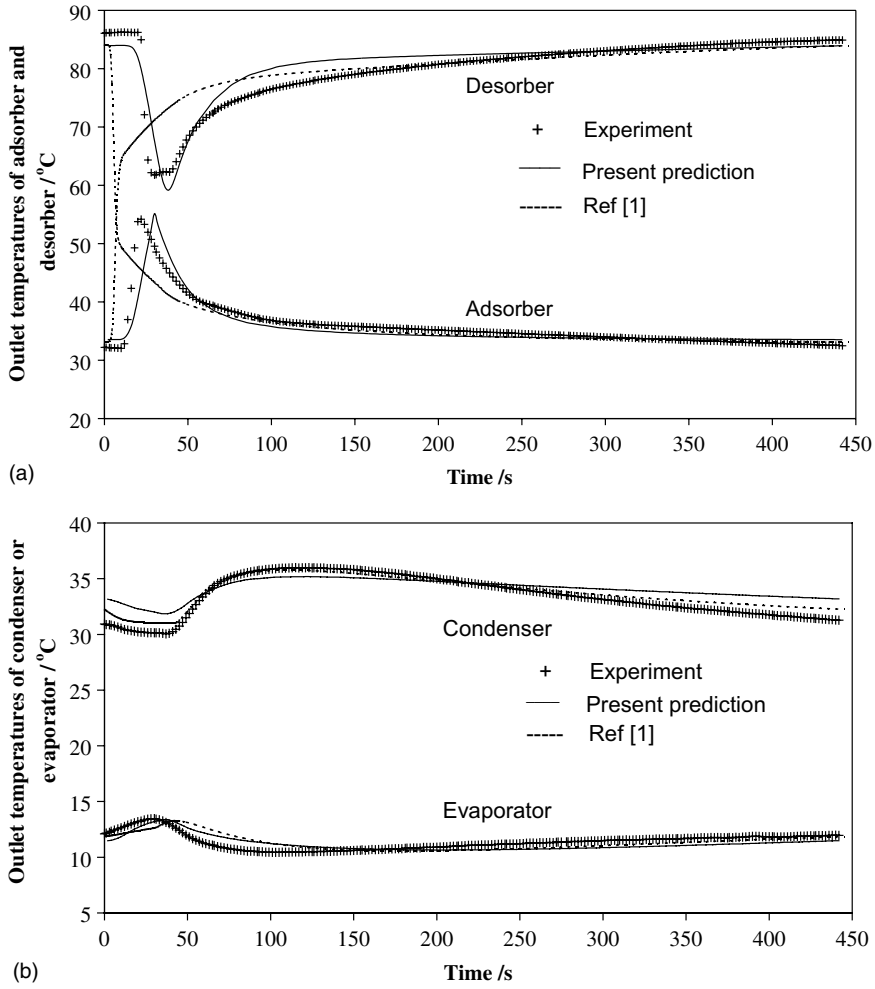

Fig. 3. (a) Simulated and experimental hot-water and cooling-water outlet temperatures from the system. (b) Simulated and experimental fluid outlet temperatures from the condenser and evaporator.

3.3. Variation of water vapor uptake of silica gel inside the adsorber

Fig. 6 shows the water uptake variation of silica gel with time in axial direction. One can clearly see that the shorter the distance of the silica gel from the heat transfer tube inlet, the faster is its adsorbed mass variation. It can also be observed that the water uptake of silica gel closer to the heat transfer tube varies quicker than those which are radially further from the heat transfer tube as shown in Fig. 7.

3.4. Effects of switching time

When the adsorber and desorber are saturated, the adsorber must be switched to the desorber for regeneration and the desorber must be switched to the adsorber to provide cooling. For the basic two-bed adsorption model, an isolated and near-isosteric thermal swing process (i.e. the switching stage) is introduced to avoid an immediate connection between the saturated cold desorber and the condenser as well as between the hot adsorber and the evaporator. Connecting the saturated cold bed immediately to the condenser will not destroy the condensing pressure since the condensate in the condenser can evaporate and easily maintain the saturated pressure. However, connecting the regenerated hot bed to the evaporator will cause a momentary desorption of adsorbate and will therefore reduce the instantaneous cooling capacity. As a result, the switching phase plays an important role on the chiller's performance and may be indispensable. Fig. 8 presents the effects of switching time on cycle average cooling capacity and the peak evaporator outlet temperature. One

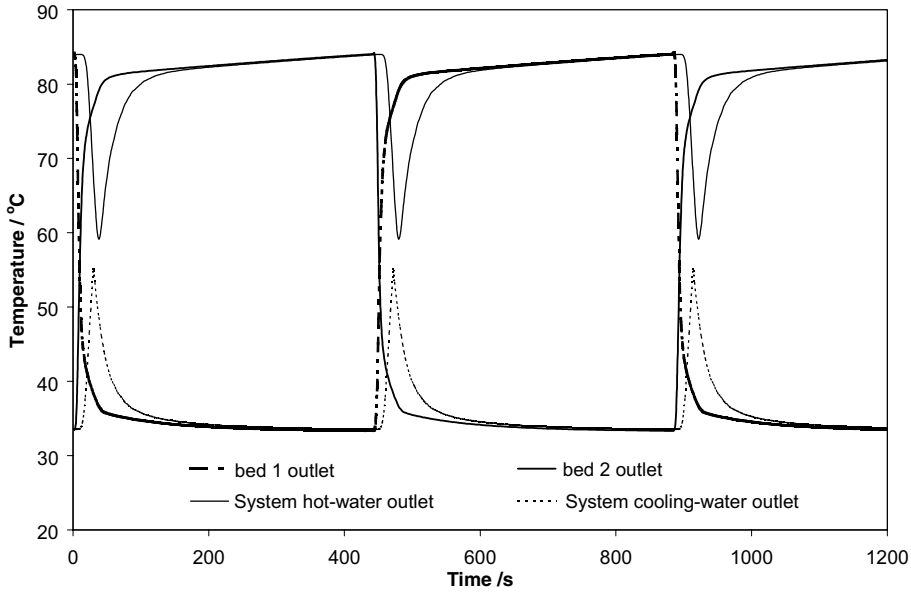

Fig. 4. A comparison of bed and system fluid outlet temperatures.

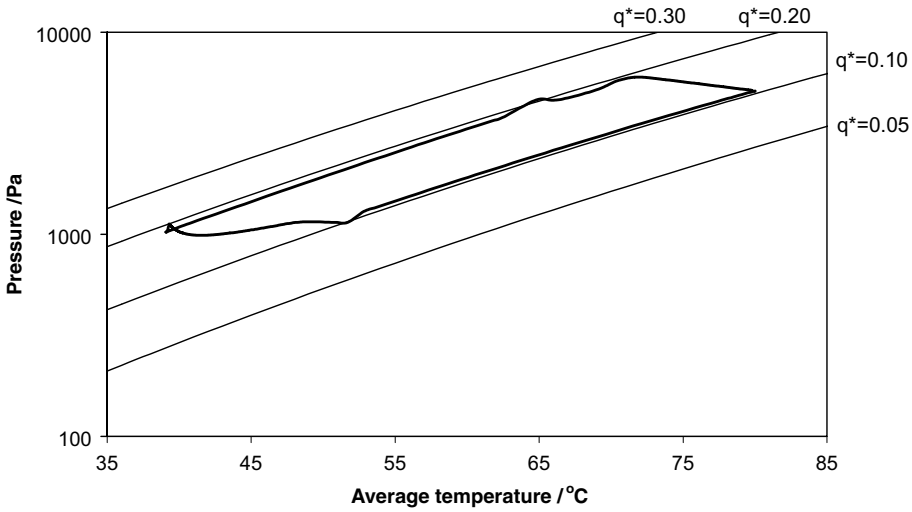

Fig. 5. Dühring diagram of the whole bed under cyclic-steady-state condition.

can observe that 35 s is the best value for the switching time. It is just a little longer than the manufacturer's selection. If we take the opening lag time of the valves into account which is typically 5 s, the manufacturer-selected 30 s switching time is more practical.

3.5. Effects of cycle time

Fig. 9 presents the effects of cycle time on COP and the cycle average chiller cooling capacity. It is clearly seen that the COP increases monotonically with the cycle time. The reason can be explained as follows. With a longer cycle time, the relative time frame occupied by bed switching which involves a significant sensible heat exchange is reduced vis-à-vis that of a shorter cycle time. This will lead to a favorable effect on the COP. The variation of cooling capacity is not monotonic. From 100 to 230 s it increases steeply, from 230 to 650 s the variation turns gentle, beyond 650 s, it begins to decrease. Lower cooling capacity under a shorter cycle time is caused by a reduced extent of adsorption, which is also related to a reduced extent of desorption due to

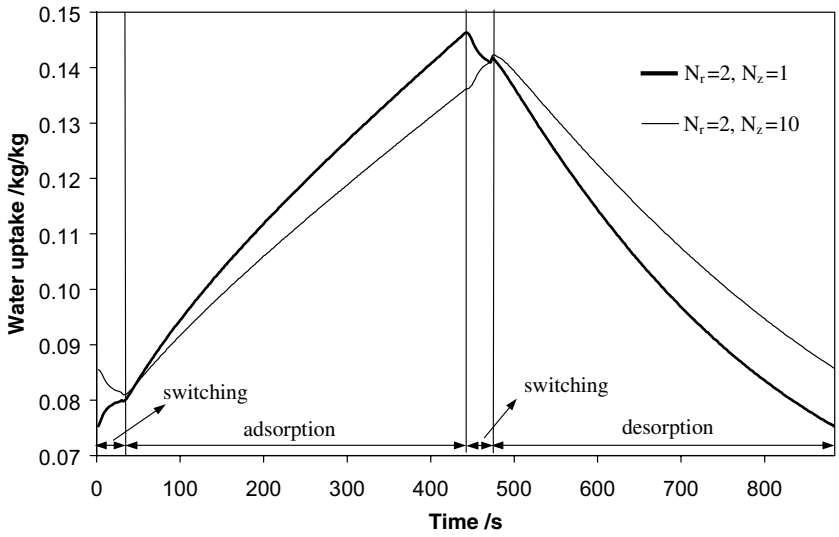

Fig. 6. Water uptake variation of silica gel with time in the axial direction.

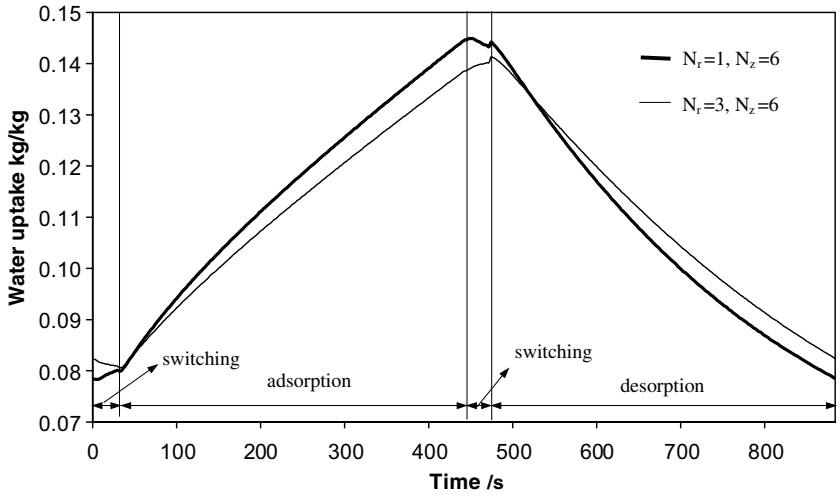

Fig. 7. Water uptake variation of silica gel with time in the radial direction.

the insufficient heating of the desorber. At a certain cycle time, the maximal adsorption–desorption capacity will be achieved at the prevailing heating and cooling water temperatures. Extending the cycle time further will not bring forth any favorable effect on useful cooling as the cycle average cooling capacity will decrease. It is also interesting to utilize the effect of cycle time to achieve part-load operation. This strategy has two advantages, viz. higher COP and easier control. We have also compared our present prediction with the previous lumped-parameter model [1]. For the lumped-parameter method which we employed earlier, the overall heat transfer coefficients of the beds are identical to those of our present model at the standard operating condition and their values do not change in other operating conditions. The effective overall U values of adsorber and desorber are 1297.3 and 1327.6 W/m^2 K, respectively. This results in an underestimation of the chiller performance at long cycle times. From Fig. 9 we confirm that if we take 850 s cycle time as an example, the previous lumped-parameter model will under-predict the cooling capacity by 14%. Since our previous model did not consider the heat recovery process and extra system coolant piping, the COPs as predicted by the lumped parameter model and our present model were not compared in this article.

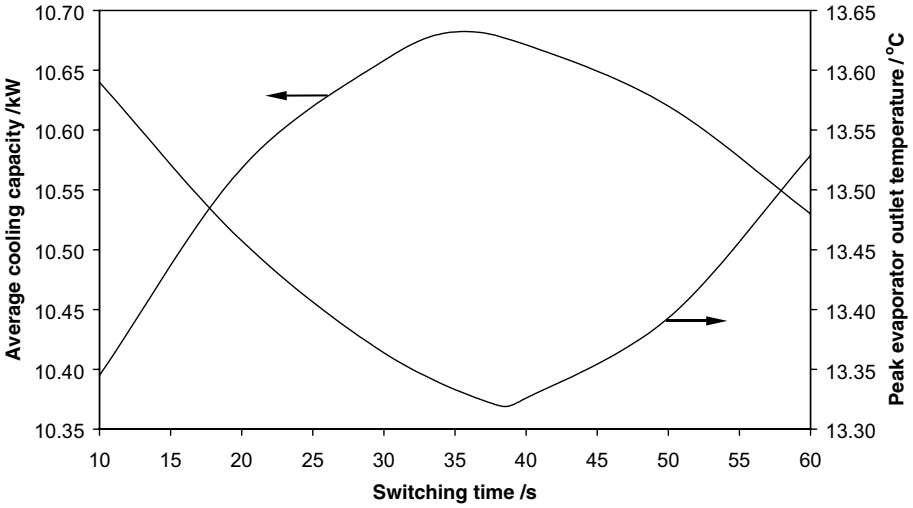

Fig. 8. Effect of switching time on average cooling capacity and peak evaporator fluid outlet temperature.

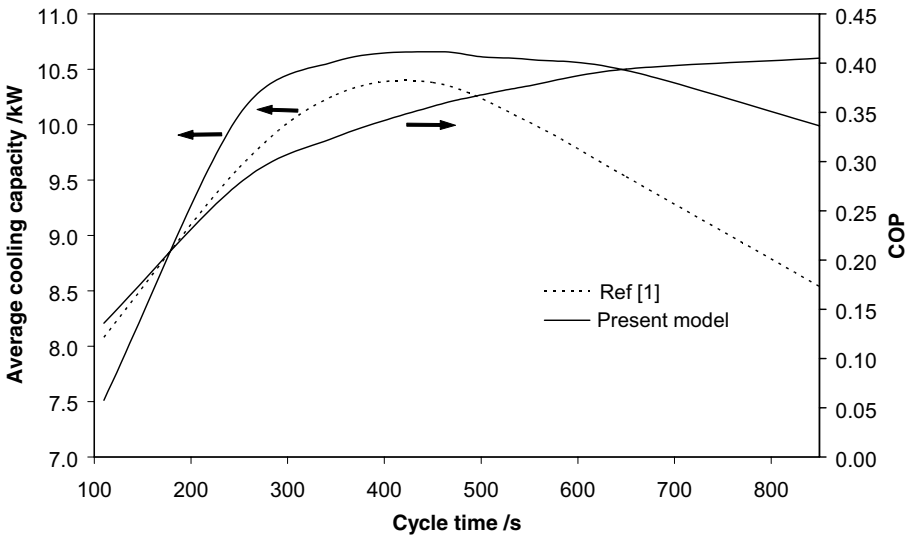

Fig. 9. Effect of cycle time on COP and cycle average cooling capacity.

4. Conclusions

We have successfully modeled the adsorption chiller cycle using a simplified 3-D, distributed-parameter approach to capture both the transient and steady state behaviors of adsorption chiller where dissipative losses in the beds have been accounted for in the simulation code. We had considered the effects on chiller performance due to a heat recovery process and the thermal buffering effect of system coolant tubes. Time constants of sensors were also considered. The simulation results agree very well with chiller experimental data.

We found that the previous lumped-parameter model tended to under-predict the cooling capacity at off-rated conditions due to its adoption of cycle-time independent heat transfer coefficients in the beds.

References

[1] H.T. Chua, K.C. Ng, A. Malek, T. Kashiwagi, A. Akisawa, B.B. Saha, Modeling the performance of two-bed, silica gel–water adsorption chillers, Int. J. Refrig. 22 (1999) 194–204.

[2] F.C. Dehler, Silica gel adsorption, Chem. Metall. Eng. 37 (1940) 307–310.

[3] E. Boelman, B.B. Saha, T. Kashiwagi, Experimental investigation of a silica gel–water adsorption refrigeration cycle-the influence of operation conditions on cooling

output and COP, ASHRAE Trans. 101 (2) (1995) 358–366.
[4] M. Karagiorgas, F. Meunier, The dynamics of a solid-adsorption heat pump connected with outside heat sources of finite capacity, J. Heat Recovery Syst. CHP 7 (1987) 85–299.
[5] N. Douss, F. Meunier, Effect of operating temperatures on the coefficient of performance of active carbon–methanol systems, J. Heat Recovery Syst. CHP 8 (1988) 383–392.
[6] E.F. Passos, J.F. Escobedo, F. Meunier, Simulation of an intermittent adsorptive solar cooling system, Solar Energy 42 (1989) 103–111.
[7] S.H. Cho, J.N. Kim, Modeling of a silica gel/water adsorption-cooling system, Energy 17 (1992) 829–839.
[8] J. Guilleminot, J.F. Meunier, J. Pakleza, Heat and mass transfer in a non-isothermal fixed bed solid adsorbent reactor: a uniform pressure non-uniform temperature case, Int. J. Heat Mass Transfer 30 (1987) 1595–1606.
[9] N.B. Amar, L.M. Sun, F. Meunier, Numerical analysis of adsorptive temperature wave regenerative heat pump, Appl. Thermal Eng. 16 (5) (1996) 405–418.
[10] L. Luo, D. Tondeur, Transient thermal study of an adsorption refrigerating machine, Adsorption 6 (2000) 93–104.
[11] L.Z. Zhang, A three-dimensional non-equilibrium model for an intermittent adsorption cooling system, Solar Energy 69 (2000) 27–35.
[12] A. Sakoda, M. Suzuki, Fundamental study on solar powered adsorption cooling system, J. Chem. Eng. Jpn. 17 (1) (1984) 52–57.
[13] J. Tóth, State equations of the solid-gas interface layers, Acta Chim. Acad. Sci. Hung. 69 (1971) 311–328.
[14] H.T. Chua, K.C. Ng, A. Chakraborty, N.M. Oo, M.A. Othman, Adsorption characteristic of silica gel + water systems, J. Chem. Eng. Data 47 (5) (2002) 1177–1181.
[15] W. Wagner, A. Kruse, Properties of Water and Steam, Springer-Verlag, New York, 1997.
[16] B.B. Saha, E.C. Boelman, T. Kashiwagi, Computer simulation of a silica gel–water adsorption refrigeration cycle—the influence of operating conditions on cooling output and COP, ASHRAE Trans. Res. 101 (2) (1995) 348–357.